Supercomputing Studies in Turbulent Rayleigh-Bénard Convection: Challenges and Perspectives

M. S. Emran, P. Götzfried, A. Kolchinskaya, J. D. Scheel, J. Schumacher

published in

NIC Symposium 2016
K. Binder, M. Müller, M. Kremer, A. Schnurpfeil (Editors)

Forschungszentrum Jülich GmbH,
John von Neumann Institute for Computing (NIC),
Schriften des Forschungszentrums Jülich, NIC Series, Vol. 48,
ISBN 978-3-95806-109-5, pp. 381.
http://hdl.handle.net/2128/9842

Supercomputing Studies in Turbulent Rayleigh-Bénard Convection: Challenges and Perspectives

Mohammad S. Emran[1], Paul Götzfried[1], Anastasiya Kolchinskaya[1], Janet D. Scheel[2], and Jörg Schumacher[1]

[1] Institute of Thermodynamics and Fluid Mechanics, Technische Universität Ilmenau, 98684 Ilmenau, Germany
E-mail: joerg.schumacher@tu-ilmenau.de

[2] Department of Physics, Occidental College, Los Angeles, California, 90041, USA

Massively parallel supercomputations are an important analysis tool to study the fundamental local and global mechanisms of heat and momentum transfer in turbulent convection. Rayleigh-Bénard convection, which evolves in a fluid layer that is uniformly heated from below and cooled from above, is the simplest setting for a buoyancy-driven turbulent flow and thus a paradigm for many turbulent flows in nature and technology. We discuss two topics of this vital field of fundamental turbulence research – large-scale pattern formation in the turbulent regime and convection at very low Prandtl numbers.

1 Introduction

Turbulent convection is an important area of present research in fluid dynamics with applications to diverse phenomena in nature and technology. They reach from chip cooling devices, heat exchangers in power plants and energy efficient indoor ventilation via convection in the Earth's atmosphere, core and oceans to convection in the Sun and other stars. Often turbulent convection is then combined with other physical processes such as rotation, electromagnetic fields or phase changes. The turbulent Rayleigh-Bénard convection (RBC) model is at the core of all these turbulent flows. It can be studied in a controlled manner, but has enough complexity to contain the key features of turbulence in heated fluids. This flow in cylindrical cells has been investigated intensively over the last few years in several laboratory experiments all over the world[1,4]. In a RBC, a fluid cell or layer is kept at a constant temperature difference $\Delta\theta = \theta_{bottom} - \theta_{top}$ between top and bottom plates which are separated by a vertical distance H. The dimensionless Rayleigh number, $Ra = CH^3\Delta\theta$, characterises the thermal driving in convective turbulence. Here $C = g\alpha/(\nu\kappa)$ with the acceleration due to gravity, g, the thermal expansion coefficient, α, the kinematic viscosity, ν, and the thermal diffusivity, κ. As the Rayleigh number keeps increasing past a critical value of 1708, a buoyancy-driven instability causes the conducting state to bifurcate via a convection state consisting of straight, parallel rolls and spatiotemporal chaotic states to an eventually fully turbulent flow. The hard turbulence regime in RBC is established for $Ra \gtrsim 10^6$. The Prandtl number $Pr = \nu/\kappa$ and the aspect ratio Γ, which is the ratio of cell diameter or cell length and cell height H, are the two other input parameters.

One of the key questions in RBC is that of the turbulent transport mechanisms of heat and momentum: How does the turbulent fluid carry heat and momentum from the heated plate at the bottom to the cold plate at the top[1,4]? In the following, we want to discuss two points which are related to this key question: the origin of large-scale flow patterns

in fully turbulent convection in extended layers and the specific turbulence properties of convection at very low Prandtl numbers. We address both points by high-resolution direct numerical simulations (DNS) in which all turbulent scales starting from the system size down to the viscous and diffusive scales which are resolved without any parametrisation or model.

The three-dimensional Boussinesq equations Eqs. 1–3 are used to model Rayleigh-Bénard convection. The first of these is the Navier-Stokes equation. The simplifying assumption is made that the density only varies linearly with the temperature in the buoyancy term. In addition we must include the heat diffusion equation and the incompressibility condition to complete our system of (dimensionless) equations:

$$\nabla \cdot \mathbf{u} = 0\,, \tag{1}$$

$$\frac{\partial \mathbf{u}}{\partial t} + (\mathbf{u}\cdot\nabla)\mathbf{u} = -\nabla p + \sqrt{\frac{Pr}{Ra}}\nabla^2\mathbf{u} + \theta\mathbf{e}_z\,, \tag{2}$$

$$\frac{\partial \theta}{\partial t} + (\mathbf{u}\cdot\nabla)\theta = \frac{1}{\sqrt{RaPr}}\nabla^2\theta\,. \tag{3}$$

The variable $\mathbf{u}(\mathbf{r},t)$ is the velocity field, $p(\mathbf{r},t)$ is the pressure, and $\theta(\mathbf{r},t)$ is the temperature. We use no-slip velocity boundary conditions along all walls. The temperature field obeys insulating sidewalls and constant values along the top and bottom plates. Alternatively to the Ra–Pr form of Eqs. 1–3, it is possible to write the Boussinesq equations with the Grashof number $Gr = Ra/Pr$ and Pr. We come back to this point in Sec. 3.

A *spectral element method (SEM)* is applied which is based on the Nek5000 software package[11]. The order of the Lagrangian interpolation polynomials which is used in each space direction is as high as $N - 1 = 13$. This code scales in our application very well up to $\sim 3 \times 10^5$ cores. Numerical details and comprehensive resolution tests are found in Scheel *et al.*[12]. The SEM is preferred if the fine-scale structure, i.e. gradients of the turbulent fields have to be analysed. A *second-order finite difference method (FDM)* for cylindrical[3,2] or Cartesian[10] nonuniform and staggered grids is additionally applied. This method has been used for the numerical investigations on the large-scale patterns which we will discuss in the subsequent section. In the cylindrical case, we can apply a two-dimensional Poisson solver after a one-dimensional fast Fourier transformation is applied in the azimuthal direction.

2 Large-Scale Circulation Patterns as Turbulent Superstructures of Convection

The classical picture is that turbulent fluid motion is characterised by a cascade of vortices and swirls of different sizes that give rise to a featureless and stochastic fluid motion. Our daily experience shows, however, that turbulent flows in nature and technology are often organised in prominent large-scale and long-living structures, which are termed *turbulent superstructures*. In convection, turbulent superstructures are mean circulation patterns whose coherence does not stop at the natural scale of the height H, but extends over much larger scales. When present, these turbulent superstructures dominate the global transport of heat and momentum. One way to answer the yet open question on their dynamical

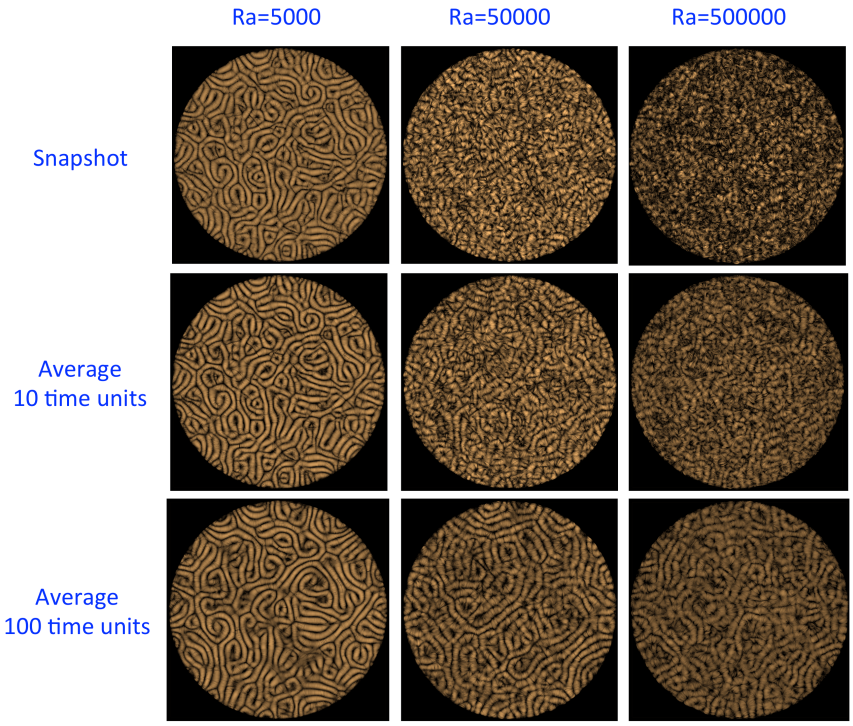

Figure 1. Top view on the velocity field patterns for cylindrical convection cells with an aspect ratio of $\Gamma = 50$. We compare a snapshot and two time averages over 10 and 100 time units T. All runs are at $Pr = 0.7$. Note that the patterns in the upper left and lower right panels of this figure almost agree.

origin is to monitor the structure formation in large aspect ratio cells starting at moderate Rayleigh numbers.

Our simulations showed that large-scale flow patterns, which are well-known from the spiral defect chaos regime of thermal convection at Rayleigh numbers $Ra < 10^4$, continue to exist in our three-dimensional numerical simulations of turbulent Rayleigh-Bénard convection in cylindrical cells with $\Gamma = 50$, $Pr = 0.7$ and $Ra \leq 5 \times 10^5$. In Fig. 1 we display the streamlines of the velocity field viewed from the top for three different Rayleigh numbers and compare instantaneous flow snapshots and time averages which have been obtained for two different intervals. At $Ra = 5000$ (left column) the convection flow is in the weakly nonlinear regime. The streamlines show that rolls are formed between the plates in a pattern of spirals and defects. Differences between a single snapshot and time averages are very small. For Rayleigh numbers $Ra = 50\,000$ (mid column) and $500\,000$ (right column) the magnitude of turbulent fluctuations exceeds the magnitude of the mean flow. Flow snapshots appear rather featureless. When the turbulent fields are averaged in time and turbulent fluctuations are thus removed, regular patterns are revealed, which we term turbulent superstructures of the convection flow[7]. On the one hand, the averaging time should be long enough such that the fluctuations are suppressed. On the other hand, this time should be smaller than the time scale on which such a large-scale

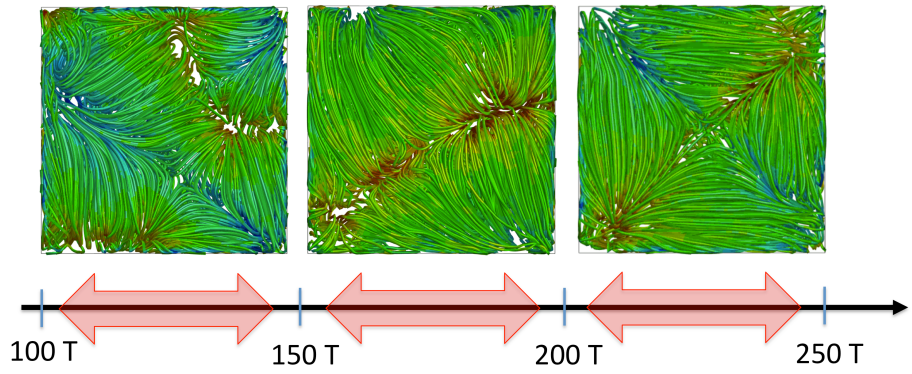

Figure 2. Top view on the mean velocity field patterns for a rectangular convection cell with $\Gamma = 3$. We compare the time averages which have been obtained over three successive intervals of 50 time units T. The run is at $Ra = 10^7$ and $Pr = 0.7$. The stream ribbons are coloured with respect to the vertical velocity (red for upwelling, green for almost zero and blue for downwelling).

pattern evolves which typically grows with $\sim \Gamma^2$.

Although the Rayleigh numbers have been moderate, the simulations are very demanding since the numerical effort grows at least with Γ^2. Our analysis proceeds in two directions: first, we study how the mean flow structure changes as the Rayleigh number is increased. These simulations have to be conducted in smaller aspect ratio cells. The numerical effort is rapidly increasing as can be seen by the DNS from Ref. 13 for $Ra = 10^8$, for example. There, we compared a run at $\Gamma = 1$ with a single large-scale circulation roll with a run at $\Gamma = 3$. The latter run has just two large-scale circulations roll, i.e., we are still far away from extended patterns as in Fig. 1. The run at $\Gamma = 1$ required $N_e = 256\,000$ spectral elements, a polynomial expansion on each cell of $N = 12$ and thus a total number of mesh cells of $N_e N^3 \approx 4.4 \times 10^8$. The run at $\Gamma = 3$ required $N_e = 2\,304\,000$, $N = 10$ and $N_e N^3 \approx 2.3 \times 10^9$. The latter run is almost 9 times bigger as the $\Gamma = 1$ run and required 32768 MPI tasks on Blue Gene/Q. These studies revealed that the local turbulent heat transport depends sensitively on the shape of the superstructures in RBC.

Secondly, rectangular cells are investigated in order to study how the formation of turbulent superstructures is influenced by the different geometry. While turbulent convection in a cylindrical cell obeys homogeneity of statistical moments in the azimuthal direction, a rectangular cell has a preferred direction which is along the diagonal. First simulation results are displayed in Fig. 2 for a Rayleigh number of 10^7. Mean patterns which have been obtained over disjoint time intervals switch between the two diagonals of the cell as visible by comparison of left and mid panels.

3 Turbulent Convection at Very Low Prandtl Numbers

Compared to the vast number of investigations at $Pr \gtrsim 1$, the very-low-Pr regime appears almost as a "terra incognita" despite many applications. Turbulent convection in the sun is present at Prandtl numbers $Pr < 10^{-3}$, in the liquid metal core of the earth one finds $Pr \sim 10^{-2}$. Convection flows as present in material processing, nuclear engineering, or

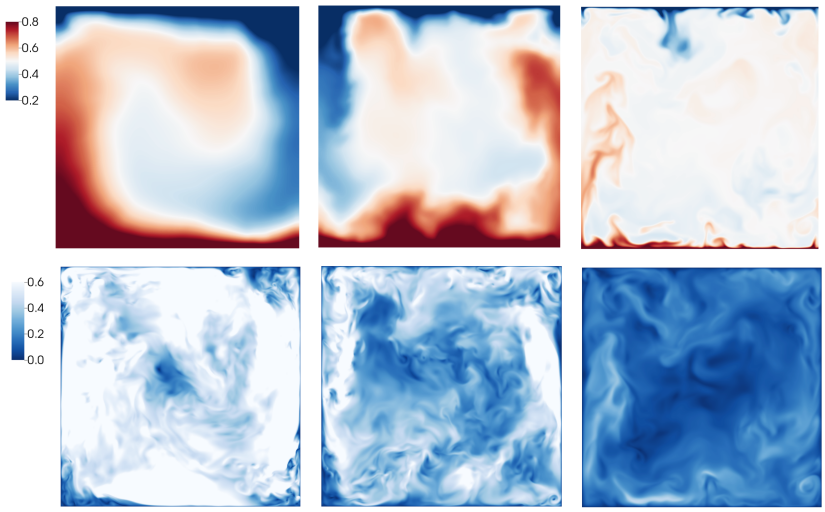

Figure 3. Vertical instantaneous cuts for the temperature field T (top row) and the magnitude of the velocity field $|\mathbf{u}|$ (bottom row). Left: $Ra = 2.38 \times 10^6$ and $Pr = 0.005$ for liquid sodium. Mid: $Ra = 10^7$ and $Pr = 0.021$ for liquid mercury. Right: $Ra = 3.33 \times 10^8$ and $Pr = 0.7$ for convection in air. All data are obtained at the same Grashof number $Gr = 4.76 \times 10^8$. The corresponding colour scales are the same.

liquid metal batteries have Prandtl numbers between 5×10^{-3} and 2×10^{-2}. One reason for significantly fewer studies of convection at low Prandtl numbers is that laboratory measurements have to be conducted in opaque liquid metals, partly operated at temperatures significantly larger than room temperature. The only way to access the statistics in these turbulent flows is via ultrasound or X-ray probes. Examples are mercury[5] or gallium at $Pr \approx 0.02 - 0.025$ and liquid sodium[8] at $Pr \approx 0.005 - 0.009$. Liquid sodium provides the lowest Prandtl number which is accessible in controlled conditions of a laboratory experiment.

Direct numerical simulations (DNS) are currently the only way to gain access to the full three-dimensional convective turbulent fields in low-Pr convection and to assure the accuracy of the boundary conditions. These simulations turn out, however, to become very demanding when the small-scale structure of turbulence has to be studied, even for moderate Rayleigh numbers Ra. To give an example: a simulation for convection in liquid sodium at $Ra = 2.38 \times 10^6$ required the same SEM mesh of 4.1×10^9 cells as a simulation for convection in air at $Ra = 10^{10}$, i.e. at a Rayleigh number that is almost four orders of magnitude larger than in sodium. Both DNS runs were conducted on 65 536 MPI tasks on BG/Q.

While the heat transport is reduced in low–Pr convection, the production of vorticity and shear are enhanced significantly. We found that this in turn amplifies the small-scale intermittency in these flows and makes them better comparable to classical Kolmogorov turbulence[14]. This result has important consequences in view to parametrisations for the small-scale turbulence in low-Prandtl-number fluids which are necessary in many applications such as in nuclear engineering or astrophysics. In Ref. 14 it was suggested that

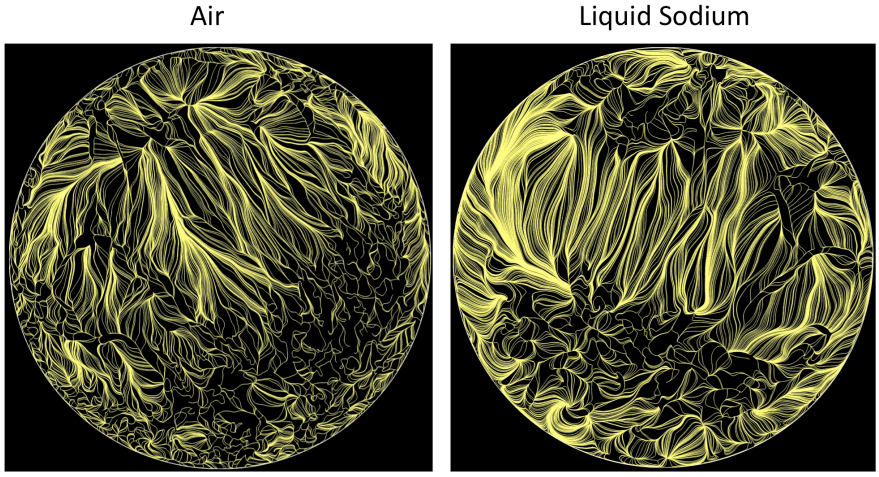

Figure 4. Field line snapshot of the skin friction field $\mathbf{s}(x, y, z = 0, t_0)$ taken at the bottom plate of the convection cell. Left: Air at $Ra = 10^{10}$ and $Pr = 0.7$. Right: Liquid sodium at $Ra = 2.38 \times 10^6$ and $Pr = 0.005$. In both figures we observe a large area fraction of the skin friction field in which the field lines are aligned.

a comparison of the fluid turbulence at different Prandtl numbers should be conducted at the same Grashof number $Gr = Ra/Pr$ rather than at a same Rayleigh number. This can be motivated by an inspection of the dimensionless momentum equation Eq. 2. If Gr is constant for different runs then Eq. 2 remains unchanged. In Fig. 3, we display vertical snapshot cuts of the temperature and the velocity magnitude for three simulations at the same Grashof number. Note that a constant Grashof number implies both, a change of Pr and Ra. With decreasing Prandtl number, the temperature field becomes increasingly washed out due to the enhanced thermal diffusivity while the velocity field is more vigorous thus indicating the enhanced level of fluid turbulence. We have shown that the cascade of the fluid turbulence is extended at the large-scale and small-scale end with decreasing Prandtl number thus enhancing the flow Reynolds number and consequently the turbulent momentum transport in the convection flow. The more vigorous fluid turbulence enhances in the enstrophy production in the fluid.

Since the Rayleigh-Bénard fluid is confined between rigid impermeable walls, tiny boundary layers of the temperature and velocity fields form in the vicinity of the walls. All the heat that is supplied by the boundary conditions has to pass these boundary layers. They form a bottleneck that constrains the global heat transport. How can this bottleneck be widened? One way is to enhance thermal diffusivity in relation to the viscosity, as done in low–Pr fluids. This certainly increases the width of the thermal boundary layer, but reduces the magnitude of the temperature gradients and thus the overall turbulent heat transfer at the same time. An alternative way is achieved when the boundary layers of velocity and temperature become fully turbulent. This regime of convective turbulence is called the *ultimate regime* of convection and goes back to a seminal paper from 1962 by Kraichnan[9]. The existence and the Rayleigh number range at which this transition into the ultimate regime proceeds is currently intensively discussed in the community.

It can however be expected that if the transition to fully turbulent boundary layers exists then the transition Rayleigh number range will depend on the Prandtl number. Our recent high-resolution DNS in the very low-Pr regime provide first hints although the accessible Rayleigh numbers are still too small. In Fig. 4 we display the velocity gradient at the heated plate at $z = 0$. The original nine-component velocity gradient tensor $A_{ij} = \partial u_i/\partial x_j$ is reduced to a two-component vector field $\mathbf{s} = (A_{13}, A_{23})$ at the wall due to the no-slip boundary conditions. Stream line snapshots of this *skin friction field* are shown for the runs at $Ra = 2.38 \times 10^6$ and 10^{10} that were mentioned above. The complexity of both instantaneous velocity boundary layers is by visual inspection very similar: in a larger area fraction the field lines are nearly parallel very similar to the skin friction field in turbulent channel flows[6]. Both velocity boundary layers display area fractions that are turbulent which we have determined by quantitative measures, such as local friction coefficients or local shear Reynolds numbers. For the very low Prandtl number run this turbulence transition should appear at a much smaller Rayleigh number. Thus the level of fluid turbulence is not only enhanced in the bulk[14] but also in the boundary layer when Pr decreases.

4 Perspectives

We have discussed two particular topics in turbulent Rayleigh-Bénard convection which are being addressed by supercomputations:

Origin of turbulent superstructures in convection: Our DNS showed that the mean flow patterns from the weakly nonlinear regime are found to continue to exist when fluctuations in the fully turbulent regime are removed. The patterns thus remain dynamically relevant. As we indicated, one open question is how the turbulent large-scale patterns will vary when the Rayleigh number is increased or the Prandtl number is changed. First studies in this direction in smaller cells have been reported in Ref. 2 and imply further modifications as Ra grows. Such transitions to new mean flow patterns could be analysed by bifurcation analysis, and modelled as phase transitions in the turbulent flow. This suggests one could apply a reduced amplitude equation formalism to describe the evolution of the large-scale patterns in the horizontal directions which are obtained by a decomposition into coarse and fine spatial scales as well as into slow and fast time scales. Computationally, a turbulent convection cell with $\Gamma = 15$ at $Pr = 0.7$ and $Ra = 10^9$ would require at least 57.6 million spectral elements (which are already feasible today with Nek5000) and thus about 10^{11} mesh cells. This requires at least 60 BG/Q racks for production jobs.

Bulk and boundary layer dynamics in liquid metal convection: We showed that the highly diffusive temperature field with coarse thermal plume structures is an efficient driver of fluid turbulence, both, in the bulk and in the boundary layers. Our DNS suggest therefore that the transition to turbulence in the boundary layers of liquid metal convection is triggered at lower Rayleigh numbers than for convection in air. Another open question is if this transition follows the same rules as in wall-bounded turbulent shear flows or if the temperature field alters the transition mechanisms. Simulations are the only approach to answer these questions since they can access the gradients of the fields in the vicinity of the walls. It is also clear that the Rayleigh number has to be increased further. For liquid gallium ($Pr = 0.021$), based on an extrapolation from our currently largest DNS at $Ra = 10^8$, we would need a mesh with 10^{10} cells for a high-resolution run at $Ra = 5\times10^8$.

Both topics demonstrate clearly that supercomputing has become an essential tool to reveal the secrets of turbulence, and especially those of turbulent convection.

Acknowledgements

The work is supported by the Deutsche Forschungsgemeinschaft within the Research Unit 1182, the Research Training Group 1567 and project SCHU 1410/18-1. We want to thank the John von Neumann Institute for Computing for the steady support with supercomputing resources that make this work possible, in particular by projects HIL07, HIL08 and HIL09. Further support was received by the PRACE Initiative and the DOE Incite program.

References

1. G. Ahlers, S. Grossmann, and D. Lohse, *Heat transfer and large scale dynamics in turbulent Rayleigh-Bénard convection*, Rev. Mod. Phys. **81**, 503–537, 2009.
2. J. Bailon-Cuba, M. S. Emran, and J. Schumacher, *Aspect ratio dependence of heat transfer and large-scale flow in turbulent convection*, J. Fluid Mech. **655**, 152-173, 2010.
3. R. Camussi and R. Verzicco, *Numerical experiments on strongly turbulent thermal convection in a slender cylindrical cell*, J. Fluid Mech. **477**, 19-49, 2003.
4. F. Chillà and J. Schumacher, *New perspectives in turbulent Rayleigh-Bénard convection*, Eur. J. Phys. E **35**, no. 58, 2012.
5. S. Cioni, S. Ciliberto, and J. Sommeria, *Strongly turbulent Rayleigh-Bénard convection in mercury: comparison with results at moderate Prandtl number*, J. Fluid Mech. **335**, 111-140, 1997.
6. M. S. Chong, J. P. Monty, C. Chin, and I. Marusic, *The topology of skin friction and surface vorticity fields in wall-bounded flows*, J. Turb. **13**, no. 6, 2012.
7. M. S. Emran and J. Schumacher, *Large-scale patterns in extended turbulent convection*, J. Fluid Mech. **776**, 96-108, 2015.
8. P. Frick, R. Khalilov, I. Kolesnichenko, A. Mamykin, V. Pakholkov, A. Pavlinov und S. Rogozhkin, *Turbulent convective heat transfer in a long cylinder with liquid sodium*, Europhys. Lett. **109**, 14002, 2015.
9. R. H. Kraichnan, *Turbulent thermal convection at arbitrary Prandtl number*, Phys. Fluids **5**, 1374-1389, 1962.
10. D. Krasnov, O. Zikanov, and T. Boeck, *Comparative study of finite difference approaches in simulation of magnetohydrodynamic turbulence at low magnetic Reynolds number*, Comput. Fluids **50**, 46–59, 2011.
11. `https://www.nek5000.mcs.anl.gov/`.
12. J. D. Scheel, M. S. Emran, and J. Schumacher, *Resolving the fine-scale structure in turbulent Rayleigh-Bénard convection*, New J. Phys. **15**, 113063, 2013.
13. J. D. Scheel and J. Schumacher, *Local boundary layer scales in turbulent Rayleigh-Bénard convection*, J. Fluid Mech. **758**, 344–373, 2014.
14. J. Schumacher, P. Götzfried, and J. D. Scheel, *Enhanced enstrophy generation for turbulent convection in low–Prandtl number fluids*, Proc. Natl. Acad. Sci. USA **112**, 9530–9535, 2015.